JOURNAL OF SOLID STATE CHEMISTRY 10, 109–115 (1974)

Electrical Conductivity and Defect Structure of Nd_2O_{3+x}

KEIJI NAITO, TOSHIHIDE TSUJI AND KATSUMI UNE

Department of Nuclear Engineering, Faculty of Engineering, Nagoya University, Furo-cho, Chikusa-ku, Nagoya, Japan

Received May 17, 1973

The electrical conductivity and departure from the stoichiometry of Nd_2O_3 have been measured over the temperature range of 900° to 1100° C and oxygen partial pressure of 1 to 10^{-16} atm. The hole conductivity of Nd_2O_3 is found to be proportional to $P_{O_2}^{1/n}$, where n are 4.6, 4.9, and 5.1 at 900°, 1000°, and 1100°C, respectively. From the oxygen partial pressure dependence of the hole conductivity, it is shown that the predominant point defects in nonstoichiometric $NdO_{1.5+x}$ are fully ionized and partially doubly ionized metal vacancies. From the thermogravimetric measurements, the departure from stoichiometry, x in $NdO_{1.5+x}$, is 2.0×10^{-3} at 1000°C and 1 atm. By combining the electrical conductivity and weight change data, it is shown that the hole mobility is 6.3×10^{-4} ($cm^2/V \cdot sec$) at 1000°C and 1 atm.

1. Introduction

The electrical conductivity of Nd_2O_3 has been measured by many investigators (*1–6*), but most of them have been limited to the temperature dependence of the electrical conductivity in air. Foëx (*5*) measured the temperature dependence of the electrical conductivity in four kinds of atmospheres such as oxygen, air, nitrogen, and hydrogen. Zyrin *et al.* (*6*) obtained the activation energy for conduction at $P_{O_2} = 0.2$ and 10^{-5} atm. Both of their results show that Nd_2O_3 is p-type semiconductor whose electrical conductivity is increasing with increasing oxygen partial pressure. From the thermoelectric power measurements it has been shown that Nd_2O_3 exhibits p-type conduction (*6*).

The nonstoichiometry and defect structure of Nd_2O_3 were first reported by Barret and Barry (*7*) who measured the oxygen uptake by powdered sample in oxygen gas and obtained the excess oxygen expressed as x in $NdO_{1.5+x}$ from 1.8×10^{-4} at 300°C to 0.4×10^{-4} at 800°C at final oxygen pressure of $1.3–1.8 \times 10^{-6}$ atm. They also found that the electrical conductivity was proportional to $P_{O_2}^{1/5}$ at 800°C in the oxygen partial pressure of 7.5×10^{-1} to 1.8×10^{-6} atm and interpreted above results in terms of a defect structure involving fully ionized oxygen interstitials. Barret and Barry, however, did not mention whether the electrical conductivity was due to electron or ion,so their electrical conductivity data need to be reexamined.

In this paper, the defect structure and departure from stoichiometry of Nd_2O_3 are to be studied by measuring the oxygen partial pressure dependence of the electrical conductivity and sample weight. Not only the hole mobility, but also formation energy of fully and doubly ionized metal vacancy and migration energy of hole are to be obtained.

2. Theory

The simple defects of the metal oxides exhibiting p-type conduction are metal vacancies or oxygen interstitials. For each model, the oxygen partial pressure dependence of the electrical conductivity of a sesquioxide is discussed by the usual Kröger and Vink notation (*8*), as follows.

2.1. Metal Vacancy Model

The formation of a doubly ionized metal vacancy, V_M'', can be described by the reaction

$$3/4O_2 \rightleftarrows 3/2O_0 + V_M'' + 2h \quad (1)$$

where O_0 is an oxygen ion on its normal site, and h is a hole. The dissociation of doubly ionized metal vacancy can be described as

$$V_M'' \rightleftarrows V_M''' + h. \quad (2)$$

If the number of defects is small and the interaction of defects is negligible, the application of the law of mass action to the Eqs. (1) and (2) leads to the Eqs. (3) and (4).

$$K_1 = [V_M''] \cdot p^2 / P_{O_2}^{3/4} \quad (3)$$

$$K_2 = [V_M'''] \cdot p / [V_M''] \quad (4)$$

where K_1 and K_2 are the equilibrium constants for the reactions (1) and (2); p is the concentration of holes; $[V_M'']$ and $(V_M''']$ are the concentration of doubly and fully ionized metal vacancies, respectively.

The electrical neutrality condition for the crystal containing holes, and doubly and fully ionized metal vacancies, is written as

$$p = 2[V_M''] + 3[V_M'''] . \quad (5)$$

From the Eqs. (3), (4) and (5), the following equation is obtained.

$$p^4 - 2K_1 \cdot p \cdot P_{O_2}^{3/4} - 3K_1 \cdot K_2 \cdot P_{O_2}^{3/4} = 0. \quad (6)$$

The relation between the hole conductivity, σ_p, and hole mobility, μ_p, is given by

$$\sigma_p = p \cdot e \cdot \mu_p. \quad (7)$$

In the case that the hole mobility is independent of defect concentration, then from the Eqs. (6) and (7), the oxygen partial pressure dependence of hole conductivity, $1/n$, is expressed as

$$\begin{aligned} 1/n &= (d\log\sigma_p / d\log P_{O_2})_T \\ &= (d\log p / d\log P_{O_2})_T \\ &= (1/4)[1 + \{1/(2Z+3)\}]^{-1} \quad (8) \\ Z &\equiv [V_M'']/[V_M''']. \end{aligned}$$

From the Eq. (8), it can be shown that in the cases of $[V_M'''] \gg [V_M'']$ and $[V_M''] \gg [V_M''']$, the oxygen partial pressure dependences of σ_p, $1/n$, are 1/5.3 and 1/4, respectively.

2.2. Oxygen Interstitial Model

The formation of a singly ionized oxygen interstitial, O_i', and doubly ionized one, O_i'', can be described by the reaction

$$1/2O_2 \rightleftarrows O_i' + h \quad (9)$$

$$O_i' \rightleftarrows O_i'' + h. \quad (10)$$

In the case of oxygen interstitial model, the following Eqs. (11), (12), (13), and (14) are obtained corresponding to the Eqs. (3), (4), (5), and (8) in the metal vacancy model, respectively.

$$K_9 = [O_i'] p / P_{O_2}^{1/2} \quad (11)$$

$$K_{10} = [O_i''] p / [O_i'] \quad (12)$$

$$p = [O_i'] + 2[O_i''] \quad (13)$$

$$\begin{aligned} 1/n &= (d\log\sigma_p / d\log P_{O_2})_T \quad (14) \\ &= (d\log p / d\log P_{O_2})_T \\ &= (1/2)[2 + \{2/(Z'+2)\}]^{-1} \\ Z' &\equiv [O_i']/[O_i''] \end{aligned}$$

where $[O_i']$ and $[O_i'']$ are the concentration of singly and doubly ionized oxygen interstitials, respectively; K_9 and K_{10} are the equilibrium constants for the reactions (9) and (10). From the Eq. (14), it can be shown that in the cases of $[O_i''] \gg [O_i']$ and $[O_i'] \gg [O_i'']$, the oxygen partial pressure dependences of σ_p, $1/n$, are 1/6 and 1/4, respectively.

In Fig. 1, $1/n$ calculated is shown against $\log Z$ or $\log Z'$.

The oxygen partial pressure dependence of the electrical conductivity and defect structure

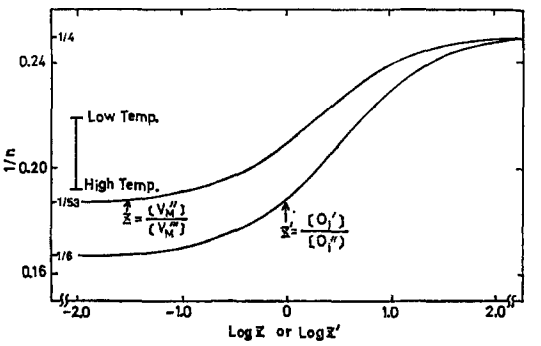

FIG. 1. Plot of $1/n$ against $\log Z$ or $\log Z'$.

TABLE I

OXYGEN PARTIAL PRESSURE DEPENDENCE OF THE ELECTRICAL CONDUCTIVITY AND DEFECT STRUCTURE OF RARE EARTH SESQUIOXIDES

Oxides	$\sigma \propto P_{O_2}^{1/n}$ (n)	Defect structure	Investigators
Nd_2O_3	5	O_i	Barrett and Barry (*7*)
	5.1 ~ 4.5	V_{Nd}	This work
La_2O_3	4	O_i	Etsell and Flengas (*9*)
	6	O_i	Rudolph (*10*)
Eu_2O_3	5.5	V_{Eu}	Schwab and Bohla (*11*)
Ho_2O_3	5.3	V_{Ho}	SuBBa Rao *et al.* (*1*)
Y_2O_3	5.33	V_Y	Tallan and Vest (*12*)

of rare earth sesquioxides which have been reported previously, including the result of this work, are summarized in Table I.

3. Experimental

3.1. Sample Preparation

The pellet for the electrical conductivity measurements was prepared by the following procedure. Nd_2O_3 powder was pressed in a 7-mm circular die at about 2 ton/cm^2 to yield a pellet 7 mm in diameter and 1.5 mm thick. Four holes of 0.3 mm in diameter were drilled in a line and a platinum wire of 0.3 mm in diameter was inserted into each hole as an electrode. The pellet was sintered in air at 1400°C for 92 hr to 80% of the the theoretical density of A-type Nd_2O_3. The platinum electrodes were fixed tightly to the pellet by sintering.

TABLE II

IMPURITY ANALYSIS OF Nd_2O_3 POWDER

Impurity	Wt. %
Y_2O_3	0.002
Pr_6O_{11}	0.002
Sm_2O_3	0.003
Dy_2O_3	<0.0025
Fe	<0.0005
Cu	<0.0001
Zn	<0.0005
Ca	0.0026
Ni	<0.0005
Si	0.0010
Co	<0.0005

The purity of the Nd_2O_3 powder used in this study was 99.99% and the result of impurity analysis is given in table II. The same Nd_2O_3 powder as used for the electrical conductivity measurements was also used for the thermogravimetric measurements.

3.2. Electrical Conductivity Measurements

The electrical conductivity measurements were carried out by means of the same conventional four inserted method as described in the previous paper (*13*). The specific resistivity, ρ, of the circular pellet is given as (*14*, *15*).

$$\rho = (2 \ln 2) \cdot s \cdot \{C_1(\phi/s)/C_2(s/w)\}(V/I) \quad (15)$$

where V is the potential drop between two probes, I is the supplied current, w and ϕ are the thickness and diameter of the pellet, and s is the spacing between adjacent probes. The specific resistivity calculated from the Eq. (15) is then converted to conductivity, σ, by the following equation to correct for the porosity (16).

$$\sigma = (1/\rho) \cdot [1 + \{f/(1 + f^{2/3})\}] \quad (16)$$

where f is the volume pore fraction of the pellet.

The schematic diagram for measuring electrical conductivity of the sample under various oxygen partial pressures is given in Fig. 2. The oxygen and water contained in CO_2, Ar, and H_2 gases were removed by passing through a copper bed at 180°C and dry ice trap, respectively. The various oxygen partial pressures were prepared by means of two methods. For the oxygen partial pressures of 1 to 10^{-6} atm, Ar—O_2 gas mixtures at a total pressure of 1 atm were used. The oxygen partial pressures in the low pressure region were obtained by introducing CO_2 and H_2 gas mixtures with known mixing ratio at a total pressure of 1 atm.

In the Ar–O_2 gas mixtures, oxygen partial pressures were determined by measuring the electrical resistance of nonstoichiometric cobaltous oxide wire at 1000°C. Oxygen partial pressure above $P_{O_2} = 10^{-3}$ atm obtained from volume ratios is in good agreement with that determined from the electrical resistance of nonstoichiometric cobaltous oxide wire at

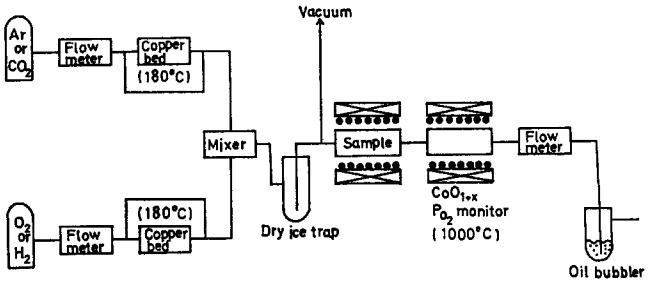

FIG. 2. Schematic diagram for measuring electrical conductivity.

1000°C. In the oxygen partial pressure below $P_{O_2} = 10^{-3}$ atm, oxygen partial pressures could not be determined from the volume ratio because of the experimental errors of flow meter and gas leak or gas generation in the system. The oxygen partial pressure dependence of the electrical resistance of CoO_{1+x} is shown in Fig. 3. In the high pressure region, $P_{O_2} > 10^{-5}$ atm, where the departure from stoichiometry is large, the relation $R/R_0 \propto P_{O_2}^{-1/4}$ (R_0; R at $P_{O_2} = 1$ atm) is found in previous works (*17–22*), but in the low pressure region, they are not in good agreement. In this experiment the oxygen partial pressure was determined from our result $R/R_0 \propto P_{O_2}^{-1/4}$ (*22*).

In the CO_2–H_2 mixtures, it was confirmed by the preliminary experiments using cobaltous oxide wire that for the flow rates from 0.25 cm/sec to 0.4 cm/sec, the equilibrium was established. For the oxygen partial pressure below 10^{-12} atm, at 1000°C, where CoO is

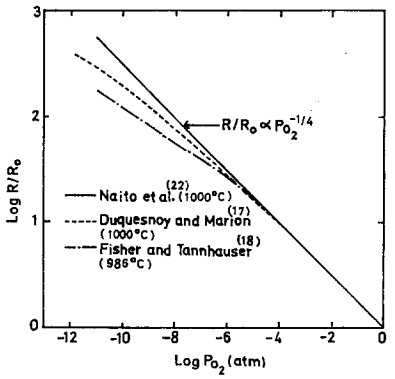

FIG. 3. Oxygen partial pressure dependence of the electrical resistance of CoO_{1+x}.

reduced to Co metal, the oxygen partial pressure was calculated from initial mixing ratio, $a = P_{CO_2}(i)/P_{H_2}(i)$. The oxygen partial pressure established by the reaction

$$CO_2 + H_2 \rightleftarrows CO + H_2O \qquad (17)$$

$$CO_2 \rightleftarrows CO + 1/2O_2 \qquad (18)$$

was generally calculated from the relation (*23, 24*)

$$\log P_{O_2} = 2\log(K_{18}/2) + 2\log[(a-1) + \sqrt{(a-1)^2 + 4a/K_{17}}] \qquad (19)$$

where K_{17} and K_{18} are the equilibrium constants for the reactions (17) and (18), respectively.

A linear flow rate of 0.3 cm/sec at room temperature was maintained for all gas mixtures used in this investigation. The temperature was measured with a Pt–Pt 13% Rh thermocouple, and the temperature of furnaces was controlled to ±2°C by electronic controller.

3.3 Thermogravimetric Measurements

For the thermogravimetric measurements, Cahn RG microbalance was set above the furnace and the sample was suspended in the hot zone of the furnace with platinum wire. The noise of thermobalance was about 12 μg as peak-to-peak. This was mainly caused by gas turbulence.

The departure from stoichiometry, x in $NdO_{1.5+x}$, can be written as

$$x = (M/2A)\cdot(\Delta W/Ws) \qquad (20)$$

where ΔW is the weight change from the stoichiometric weight, Ws, which was found

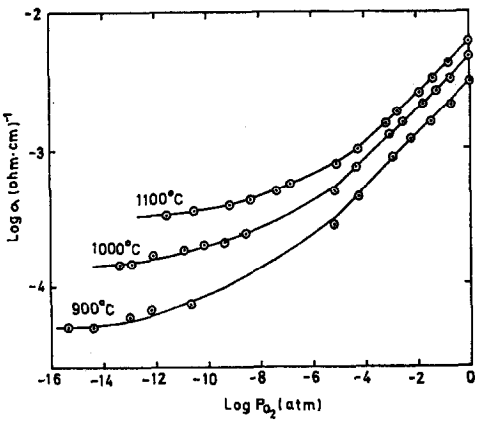

FIG. 4. Electrical conductivity of Nd_2O_3 as a function of oxygen partial pressure from 900° to 1100°C.

by extrapolating the sample weight to $P_{O_2} = 0$ at each temperature, M is the molecular weight of Nd_2O_3 and A is the atomic weight of oxygen.

4. Results and Discussion

4.1. Defect Structure

The electrical conductivity of Nd_2O_3 as a function of oxygen partial pressure from 900° to 1100°C is shown in Fig. 4. As seen in Fig. 4, p-type conduction exists over the high pressure region. The p-type behavior was also verified by the thermoelectric power measurements at high oxygen partial pressures (*6*, *27*). However the contribution of p-type conduction is becoming smaller with decreasing oxygen partial pressure. Probably, in the low pressure region near the stoichiometry of Nd_2O_3, the ionic conduction which is independent of oxygen partial pressure may contribute predominatly to the conductivity measured. From galvanic cell measurements, it has been reported that Nd_2O_3 is ionic conductor in the low pressure region (*25*). Therefore, total conductivity, σ_t, can be expressed as the sum of electronic conductivity, σ_p, and ionic one, σ_i,

$$\sigma_t = \sigma_t + \sigma_p \qquad (21)$$

and σ_p is obtained by substracting σ_i from σ_t. The value of σ_i which gives the best linear relationship in the plot of log σ_p vs. log P_{O_2} is obtained for each temperature.

The oxygen partial pressure dependence of the hole conductivity, σ_p, at 1100°C is shown in Fig. 5. The slopes of the plot of log σ_p vs. log P_{O_2}, $1/n$, are given for each temperature in Table III. From Table III, it is seen that the value of n is varied from 5.1 at 1100°C to 4.6 at 900°C. As the value of n at high temperature is near to 5.3, it can be considered from Fig. 1 that the predominant defects at high temperature are fully ionized metal vacancies. It is also expected that the contribution of doubly ionized metal vacancies increase with decreasing temperature, since the value of n gradually approaches 4 at low temperatures as seen in Table III.

Barret and Barry (*7*) found the relationship $\sigma \propto P_{O_2}^{1/5}$ from the electrical conductivity measurements of Nd_2O_3 at 800°C and oxygen partial pressure of 7.5×10^{-1} to 1.8×10^{-6} atm, and interpreted their results in terms of a defect structure involving fully ionized oxygen interstitials. However, as shown in Fig. 1, it may be more reasonable to conclude that the defect structure is fully ionized metal vacancies rather than fully ionized oxygen interstitials.

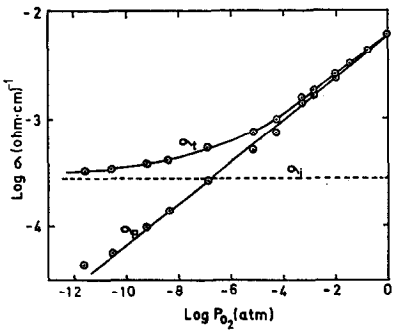

FIG. 5. Electrical conductivities of Nd_2O_3 at 1100°C.

4.2. Defect Concentration

The relation between the departure from stoichiometry, x, and vacancy concentration is expressed as

$$x = 3/2([V_M''] + [V_M'''])(M/N_0 d) \qquad (22)$$

where d is the density of Nd_2O_3 and N_0 is Avogadro's number. From $Z \equiv [V_M'']/[V_M''']$ and Eqns. (5) and (22), x is written by

$$x = (3p/2)\cdot\{(Z+1)/(2Z+3)\}(M/N_0 d). \qquad (23)$$

TABLE III

OXYGEN PARTIAL PRESSURE DEPENDENCE OF THE HOLE CONDUCTIVITY (n in $\sigma_p \propto P_{O_2}^{1/n}$)

T(°C)	900	950	1000	1050	1100
n	4.6 ± 0.2	4.5 ± 0.2	4.9 ± 0.2	4.9 ± 0.2	5.1 ± 0.2

The oxygen partial pressure dependence of the departure from stoichiometry, is expressed from the Eqs. (8) and (23) as

$$(d\log x/d\log P_{O_2})_T = (d\log p/d\log P_{O_2})_T = (d\log \sigma_p/d\log P_{O_2})_T = 1/n. \quad (24)$$

Therefore, when σ_p is proportional to $P_{O_2}^{1/n}$, the departure from stoichiometry, x, is also proportional to $P_{O_2}^{1/n}$. In Fig. 6, the relative weight changes, ΔW, as well as departure from stoichiometry are plotted as a function of $P_{O_2}^{1/n}$ using the value of n shown in Table III. As seen in Fig. 6, the departure from stoichiometry, x in $NdO_{1.5+x}$, is 2.0×10^{-3} at 1000°C and 1 atm, and x increases with increasing temperature at constant oxygen partial pressure. This is, however, not in agreement with Barret and Barry's result where x decreases with increasing temperature. As the departure from stoichiometry usually increases with increasing temperature in oxides, it is a question whether their result represents the bulk properties of the oxide.

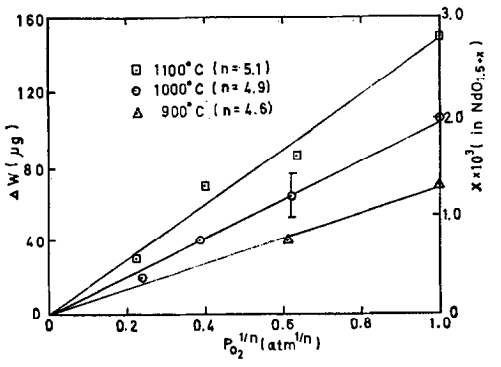

FIG. 6. Relative weight changes and departure from stoichiometry as a function of $P_{O_2}^{1/n}$.

4.3. Hole Mobility

From the Eqs. (7) and (23), the hole mobility, μ_p, of Nd_2O_3 is expressed as

$$\mu_p = \sigma_p/p \cdot e = (3 \cdot \sigma_p/2x \cdot e)\{(Z+1)/(2Z+3)\}(M/N_0 d) \quad (25)$$

where Z is obtained from Fig. 1 using the value of n shown in Table III. The hole mobilities of Nd_2O_3 calculated from the thermogravimetric and electrical conductivity data at $P_{O_2} = 1$ atm are 6.3×10^{-4}, 6.3×10^{-4}, and 6.0×10^{-4} ($cm^2/V \cdot sec$) at 900°, 1000°, and 1100°C, respectively. These values are so small that the small polaron model of activated hopping motion offers the best possibility for charge transport mechanism.

4.4. Activation Energy

In Fig. 7, $\log \sigma T$ is plotted against $1/T$ at constant oxygen partial pressures considering the small polaron model of activated hopping model. From the slopes of the Arrhenius plot in Fig. 7, the activation energy for conduction can be calculated.

In the oxygen partial pressure range of 1 to 10^{-5} atm, where the hole conduction predominates over the ionic conduction as shown in Fig. 5, the activation energy is obtained as 0.54 ev. The activation energies of Nd_2O_3 obtained from the slope of the plot of $\log \sigma$ vs. $1/T$ in air have been reported by Zyrin et al. (6) and Bogroditskii *et al.* (4) as 0.64 and

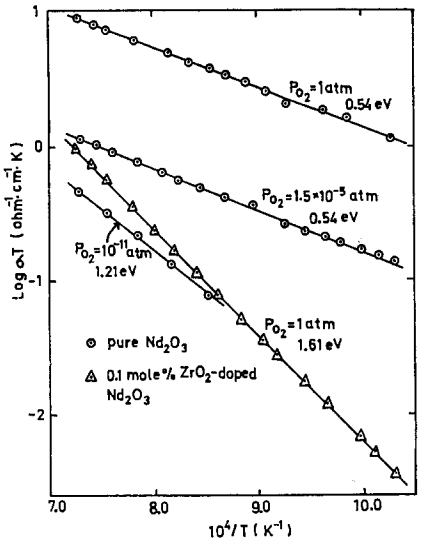

FIG. 7. Plots of $\log \sigma T$ against $1/T$ at constant oxygen partial pressures.

2.24 ev, respectively. Since the plot of $\log \sigma T$ against $1/T$ does not give the difference larger than 0.09 ev compared with the plot of $\log \sigma$ against $1/T$, the differences among the data reported may be thus caused from the impurities of sample. To substantiate above supposition, we doped 0.1 mol% ZrO_2 to Nd_2O_3 sample, then the activation energy of doped sample became to 1.61 ev as shown in Fig. 7. Accordingly, the activation energy for conduction in Nd_2O_3 is significantly affected by the existence of cation impurities.

The activation energy obtained in the oxygen partial pressure range of 1 to 10^{-5} atm is regarded as the sum of the migration energy of hole and the apparent formation energy of fully and doubly ionized metal vacancies.

In the range, $P_{O_2} < 10^{-5}$ atm, as shown in Fig. 7, the activation energy increases from 0.54 ev at $P_{O_2} = 1.5 \times 10^{-5}$ atm to 1.21 ev at $P_{O_2} = 10^{-11}$ atm, where the ionic conduction predominates over the hole conduction as shown in Fig. 5. The value of 1.21 ev is in good agreement with the activation energy for self-diffusion of oxygen ion in Nd_2O_3, 1.35 ev, reported by Stone *et al.* (*26*), so perhaps, this value corresponds to the activation energy for ionic conduction.

References

1. G. V. S. RAO, S. RAMDAS, R. N. MEHROTRA, AND C. N. R. RAO, *J. Solid State Chem.* **2**, 377 (1970).
2. R. N. MEHROTA, G. V. CHANDRASHEKAR, C. N. R. RAO, AND E. C. SUBBARAO, *Trans. Faraday Soc.* **62**, 3586 (1966).
3. V. W. NODDACK AND H. WALCH, *Z. Electrochem.* **63**, 269 (1959).
4. N. P. BOGRODITSKII, V. V. PASYNKOV, R. R. BUSILI, AND YU. M. VOLOKOBRINSKI, *Dokl. Akad. Nauk. SSSR* **160**, 578 (1965).
5. M FOËX, *C. R. Acad. Sci. Paris* **220**, 359 (1945).
6. A. V. ZYRIN, V. A. DUBOK, AND S. G. TRESVYATSKII, *in* "Chemistry of High Temperature Material" (N. A. Toropov, Ed.), p. 63. Consultants Bureau, New York, 1969.
7. M. F. BARRET AND T. I. BARRY, *J. Inorg. Nucl. Chem.* **27**, 1483 (1965).
8. F. A. KRÖGER AND H. J. VINK, "Solid State Physics" (F. Seitz and D. Turnbull, eds.) Vol. 3, p. 588. Academic Press, New York, 1956.
9. T. H. ETSELL AND S. N. FLENGAS, *J. Electrochem. Soc.* **116**, 771 (1969).
10. V. J. RUDOLPH, *Z. Naturforsch.* **A 14**, 727 (1959).
11. G. M. SCHWAB AND F. BOHLA, *Z. Naturforsch* **A 23**, 1549 (1968).
12. N. M. TALLAN AND R. W. VEST, *J. Amer. Ceram. Soc.* **49**, 401 (1966).
13. T. ISHII, K. NAITO AND K. OSHIMA, *J. Nucl. Mater.* **35**, 335 (1970).
14. A. UHLIR JR., *Bell System Tech. J.* **34**, 105 (1955).
15. F. M. SMITS, *Bell System Tech. J.* **37**, 771 (1958).
16. H. W. RUSSEL, *J. Amer. Ceram. Soc.* **18**, 1 (1935).
17. A. DUQUESNOY AND F. MARION, *C. R. Acad. Sci. Paris* **256**, 2862 (1963).
18. B. FISHER AND D. S. TANNHAUSER, *J. Chem. Phys.* **44**, 1663 (1966).
19. I. BRANSKY AND J. M. WIMMER, *J. Phys. Chem. Solids* **33**, 801 (1972).
20. N. G. EROR AND J. B. WAGNER, *J. Phys. Chem. Solids* **29**, 1597 (1968).
21. A. I. SHELYKH, K. S. ARTEMOV, AND V. E. SHVARKOUSKII, *Soviet Phys. Solid State* **8**, 706 (1966).
22. K. NAITO, N. KAMEGASHIRA, AND T. YUTANI, unpublished work.
23. L. S. DARKEN AND K. W. GURRY, *J. Amer. Chem. Soc.* **67**, 1398 (1945).
24. T. KATSURA AND M. HASEGAWA, *Bull. Chem. Soc. Japan* **40**, 561 (1967).
25. H. SCHMALZRIED, *Z. Phys. Chem.* (*NF*) **38**, 87 (1963).
26. G. D. STONE, G. R. WEBER AND L. EYRING, *Nat. Bur. Stand.* (*U.S.*), *Spec. Publ.* **296**, 179 (1968).
27. K. NAITO, T. TSUJI, AND K. UNE, unpublished work